Influence of piezoelectric parameters on admittance diagnostic signals for structural health monitoring: a numerical study

Akshay S.K. Naidu*

Department of Civil Engineering,
Methodist College of Engineering and Technology,
Hyderabad, 500001, India
Email: akshaynaidu@methodist.edu.in
and
Affiliated to: Osmania University,
Hyderabad, India
*Corresponding author

Vinay Pittala

Department of Civil Engineering,
Institute of Aeronautical Engineering,
Dundigal, Hyderabad, 500043, India
and
Affiliated to: JNT University,
Hyderabad, India
Email: vinaykumar9490@gmail.com

Abstract: The electromechanical impedance (EMI) technique for structural health monitoring (SHM) relies on the analysis of the electrical admittance response, known as the admittance signature, of a piezoelectric ceramic (PZT) chip bonded on or embedded within a structure. Damage in the structure alters its mechanical impedance. Owing to the dynamic coupling that exists between the mechanical impedances of the structure and the PZT chip, this is in turn reflected in the changed admittance signature. The changes in the admittance signature due to deterioration of the PZT characteristics need to be distinguished from those due to structural damage for effective SHM. This paper presents the results of a numerical study carried out to understand the influence of PZT material parameters and geometric characteristics on the admittance signature, which may be useful for effective analysis of diagnostic signals for SHM purposes.

Keywords: structural health monitoring; SHM; piezoelectric material; lead zirconate titanate; PZT; electromechanical impedance; EMI; admittance signatures; coupled field FE analysis.

Reference to this paper should be made as follows: Naidu, A.S.K. and Pittala, V. (2018) 'Influence of piezoelectric parameters on admittance diagnostic signals for structural health monitoring: a numerical study', *Int. J. Materials and Structural Integrity*, Vol. 12, No. 4, pp.316–338.

Biographical notes: Akshay S.K. Naidu is presently working as an Associate Professor in the Department of Civil Engineering, Methodist College of Engineering and Technology, Hyderabad, India. He obtained his BTech degree in Civil Engineering from IIT-Delhi in 1997, Master of Engineering degree from the National University of Singapore in 2000 and PhD degree from the Nanyang Technological University, Singapore in 2004. He has published several technical papers in international journals and reputed conferences, some of which are highly cited. His research interests include structural health monitoring using piezoelectric transducers, smart materials and systems, repair and retrofitting of structures and green buildings.

Vinay Pittala is presently working as an Assistant Professor in the Department of Civil Engineering, Institute of Aeronautical Engineering, Hyderabad, India. He obtained his BTech in Civil Engineering in 2014 and MTech in Structural Engineering in 2017 from Jawaharlal Nehru Technological University (JNTU), Hyderabad. His research interests include structural health monitoring using piezoelectric transducers, structural analysis and design, repair and retrofitting of structures.

1 Introduction

Early identification of damage and deterioration in structures is vital to prevent any catastrophic failures, and associated loss of lives, property and economy. Timely and effective assessment can greatly aid in adopting a cheaper and suitable structural retrofitting measures. The conventional methods of the structural condition assessment by visual inspections and localised NDT techniques, although very effective for specific situations, have certain crucial limitations. Firstly, the investigations can be carried out only at certain fixed intervals of time and not have the possibility of continuous monitoring. Secondly, these methods require expert and skilled professional human intervention for its execution. Thirdly, most of the NDT methods require that the probable location of the damage must be intuitively ascertained by the expert inspector, even before performing the diagnostics tests at that location (Bhalla, 2004; Hoła and Schabowicz, 2010). The structural health monitoring (SHM) philosophy aims at overcoming these limitations through continuous monitoring and evaluation of structural integrity by adopting a sophisticated sensing technology. The SHM methods seek to evaluate the structure globally and thus do not require the knowledge of the damage location *a priori*. These methods are intended to be applicable even during the service period of the structure (Boller and Meyendorf, 2008; Chang, 1999; Farrar and Worden, 2007). The key components of a SHM system are:

a sensing technology

b diagnostic signal generation

c data transmission and storage mechanisms

d diagnostic signal analysis

e structural assessment metric.

Numerous techniques in SHM have been developed in each of these components (Brownjohn, 2007; Diamanti and Soutis, 2010; Sohn et al., 2004).

The electromechanical impedance (EMI) technique using piezoelectric ceramic chips, which serve as self-sensing actuators, has promising features for SHM applications. Piezoelectric ceramic materials, such as lead zirconate titanate (PZT), upon application of an electric field along their polarised direction, experience mechanical strains in a perpendicular plane. Conversely, upon application of mechanical strains in the plane, produce voltage across their electrodes. This bifunctional property makes the PZT ceramic chip be used both as actuators and sensors, simultaneously. In the EMI technique, the PZT ceramic chip is either surface-bonded or embedded within a structural member at a critical location. Alternating voltage of 1 V is typically applied across the PZT electrodes at a high frequency range, which produces a high frequency vibration of the PZT chip with amplitudes in the order of micro strain. The PZT chip, in turn, induces actuation in the structure, locally. If the bond between the PZT chip and the structure is strong, there exists a coupling between the mechanical impedances of the PZT chip and the structure, which is reflected in the electrical impedance or its reciprocal, the admittance response of the PZT chip at every frequency (Liang et al., 1994a). This frequency response curve of the electrical admittance (Y) of the PZT chip is popularly known as the electromechanical admittance signature, which serves as the diagnostic signal for SHM. The admittance signature of the PZT chip, with its real and imaginary components viz. conductance (G) and susceptance (B), is measured directly by an impedance analyser (HP 4192/4194 A) or an LCR meter (Agilent E4980A Precision LCR metre). Damage or any deterioration in the structure, changes the dynamic characteristics and thus the impedance of the structure, which reflects in the change of the pattern of the admittance signature of the PZT chip. Several successful experimental verifications of the EMI technique and related technical investigations have been reviewed in detail (Park et al., 2003; Annamdas and Soh, 2010; Yan and Chen, 2010; Annamdas and Radhika, 2013; Na and Baek, 2018). Among the recent developments in the research of the EMI technique are the monitoring of hydration in concrete (Talakokula et al., 2018) and estimation of strength development in cementitious materials (Lu et al., 2017), detection of weak bonding and delamination in FRP laminates for retrofitting applications in concrete structures (Park et al., 2011; Malinowski et al., 2015; Li et al., 2017; Roth and Giurgiutiu, 2017), monitoring the integrity of pre-stressed systems (Min et al., 2016), the dual PZT model for EMI method (Adhikari and Bhalla, 2018; Song et al., 2013; Wang et al., 2016) and several damage detection applications (Tinoco et al., 2016; Liu et al., 2017; Fan et al., 2018a, 2018b, 2018c).

Researchers have derived several analytical or semi-analytical models of the EMI technique and validated them against experimental investigations. A full numerical simulation of the EMI technique has also been demonstrated by adopting the coupled field finite element (FE) analysis in ANSYS^{TM} (Liu and Giurgiutiu, 2007; Yang et al., 2008). This was further used to study the effect of axial loads (Lim and Soh, 2012). Using this numerical simulation, the admittance signatures can be directly obtained for any structural model. By adjusting the various material parameters, a close match of the numerically simulated admittance signatures with those experimentally obtained has been verified (Lim and Soh, 2014). Thus, the coupled field FE simulations of the EMI technique prove useful in further analyses that may be cumbersome to execute experimentally. A series of interesting numerical simulation results studying the effects on the real part of impedance signatures due to the FE mesh size, shape and thickness of

the PZT chip, the thickness of the bonding layer, distance of the damage notch from the PZT and decoupling of effects of loads and temperatures, have also been investigated (Djemana and Hrairi, 2016).

In this paper, the coupled field FE analysis of the EMI technique is adopted to study the influence of the electro-mechanical properties and the geometric size of the PZT ceramic chip on the admittance signature. A good understanding of the changes in patterns of the admittance signature is essential to differentiate the factual damages in the structure from the damages/deterioration of the PZT chip. Some parts of the FE simulations have been carried out by previous researchers (Lim and Soh, 2014; Djemana and Hrairi, 2016). However, this work is specific to changes in both real and imaginary parts of the admittance signatures, and gives graphical insights into the qualitative signature pattern changes. This work will be helpful in diagnostic signal analysis for EMI-based SHM and also in further studies in designing and optimisation of the SHM system.

2 Modelling of the EMI technique

Modelling of the EMI technique is vital to have a better understanding of its functioning as well as to achieve an efficient design. Various analytical, semi-analytical and numerical models simulating the PZT-structure interaction have been developed which are briefly described.

2.1 Analytical models

After several attempts to simulate the PZT-structure interaction analytically, the first effective model to capture the dynamics of the problem was the EMI model (Liang et al., 1994a). The impedance model could predict the PZT force imparted on the structure as a function of frequency more accurately than the other models (Lalande, 1995). In their impedance model, Liang et al. (1994a, 1994b) simplify the host structure into a single degree of freedom spring-mass-damper system. The entire structure can be represented by its drive point mechanical impedance, Z, resembling a black box. Incorporating the dynamic force equilibrium and PZT constitutive equations, Liang et al. (1994b) derived the following expression for the 1D electro-mechanical admittance (Y):

$$Y = \omega j \frac{w_a l_a}{h_a}\left[\overline{\varepsilon_{33}^{T}} + \left(\frac{Z_a}{Z+Z_a}\right) d_{32}^2 \overline{Y_{22}^{E}} \left(\frac{\tan kl_a}{kl_a}\right) - d_{32}^2 \overline{Y_{22}^{E}}\right] \tag{1}$$

where w_a, l_a and h_a represent the PZT width, length and thickness, respectively. ω is the angular frequency of the applied alternating voltage, Z is the mechanical impedance of the host structure, and Z_a is the mechanical impedance of the PZT chip, $\overline{\varepsilon_{33}^{T}}$ and d_{32} are piezoelectric relative permittivity and strain coefficient and $\overline{Y_{22}^{E}}$ is the complex Young's modulus.

At low frequencies, about less than 1/5th of the first resonant frequency of the PZT chip, the term $\frac{\tan(kl_a)}{kl_a} \to 1$. Adopting this quasi-static sensor approximation (Bhalla,

2004; Giurgiutiu and Zagrai, 2002; Liang et al., 1994b), the electro-mechanical admittance Y in equation (1) can be simplified as:

$$Y = \omega j \frac{w_a l_a}{h_a}\left[\overline{\varepsilon_{33}^T} - \left(\frac{Z}{Z+Z_a}\right) d_{32}^2 \overline{Y_{22}^E}\right] \tag{2}$$

Now we can write the complex relative permittivity and complex Young's modulus as $\overline{\varepsilon_{33}^T} = \varepsilon_{33}^T(1-\delta j)$ and $\overline{Y_{22}^E} = Y_{22}^E(1+\eta j)$, respectively, where δ is the dielectric loss factor and η is the mechanical loss factor for the PZT chip. We can also write the angular frequency in terms of cyclic frequency as $\omega = 2\pi f$. Substituting these in equation (2) and splitting the terms we can rewrite equation (2) as:

$$Y = 2\pi f \; j\left(\frac{w_a l_a}{h_a}\right)\left[\varepsilon_{33}^T(1-\delta j) - \left(\frac{Z}{Z+Z_a}\right) d_{32}^2 \; Y_{22}^E(1+\eta j)\right] \tag{3}$$

We can observe that the term outside the square brackets are frequency of excitation f and purely PZT geometric parameters $\left(\frac{w_a l_a}{h_a}\right)$. The first term in the square bracket deals with the relative permittivity of the PZT. The second term inside the square brackets represents the mechanical parameters of the PZT and the structure.

After the first development of the impedance model by Liang et al. (1994a, 1994b) and Zhou et al. (1996) extended Liang's model by considering 2D actuation of the PZT chip and included cross-impedances in the model. This model was applied to thin plates and shells. Giurgiutiu and Zagrai (2000) proposed a further variation of the model for dynamics of the PZT chip with an elastically constrained boundary condition using a pair of springs (dynamic stiffness) at both ends of the PZT chip. Zagrai and Giurgiutiu (2001a, 2001b, 2001c) later developed analytical models for 2D simple structures with axis-symmetry, and applied for damage identification for thin walled structures.

2.2 Semi-analytical models

In Liang's equation (1), the expressions for PZT actuator impedance (Z_a) and the drive-point structural impedance (Z) are given as input to evaluate the electrical admittance, Y. For simple 1D system models this was not difficult. For Zhou et al.'s (1996) model cross-impedance terms had to be inserted in the equation, which made the analysis very difficult. For more complicated structures, finding analytical expressions for drive-point structural impedance is practically impossible. Thus, for complicated structures mounted with a PZT, semi-analytical models were considered. In this approach, the PZT was modelled like in Liang's model, but the dynamics of the contact between PZT and the structure was limited to the numerical values of the mechanical impedance of the structure, Z, instead of an analytical expression. To get the numerical values of Z, a FE model of the structure alone, without the PZT chip, is considered. Using harmonic analysis in ANSYS^{TM} at the point where PZT is expected to contact the structure, a harmonic forcing function is applied. The ratio of the harmonic forcing function to the velocity response at the same point gives the drive-point mechanical impedance of the structure, Z, for every frequency. This Z is given as input into the

Liang's equation for 1D applications or other 2D equations developed later (Bhalla, 2004).

Fairweather (1998) developed a semi-analytical FE-based impedance model for predicting the structural response of PZT induced actuation. FE analysis was utilised to determine the host structure's impedance. Bhalla and Soh (2004a, 2004b) simplified Zhou's 2D cross-impedance model by introducing the concept of 'effective impedance', which considered the interaction between the PZT and the structure as not restricted at the two end points but extended all over edge of the PZT patch. The effective impedance was evaluated by FE analysis. Annamdas and Soh (2007) extended this concept to include 3D actuation effects of the PZT chip and introduced the 'directional sum impedance' concept in the model. A few variations of these models that were developed are summarised in detail by Lim (2007) and Lim and Soh (2014). Many researchers also included the shear lag effects due to the adhesive layer in their models (Bhalla and Moharana, 2013; Bhalla and Soh, 2004c; Madhav and Soh, 2007; Xu and Liu, 2002).

2.3 Numerical modelling

Despite the ability of analytical models to simulate the PZT-structure interaction, the solution is limited to simple structures with simple geometries and boundary conditions. When the structure to be studied is relatively complex or with complicated boundary conditions, or when the targeted model involves a system of structures interacting with each other, analytical modelling and a closed form solution is usually impossible. Semi-analytical models are also limited as the contact between the PZT and structure is assumed to be at the PZT edges only, thus failing to capture the full PZT-structure dynamic interaction.

The coupled-field FE analysis using ANSYS^{TM} provides full numerical modelling of the EMI technique for SHM. Liu and Giurgiutiu (2007) first compared the real impedances from the FE-based impedance model (non-coupled) and coupled field model for a 1D narrow beam structure with those of the experimental tests. The coupled field FE model solutions had closer agreement to the experimental results. Yang et al. (2008) demonstrated the ability of the coupled-field FE model in simulating the PZT-structure interaction with good agreement of the resonant frequencies with the experimental results up to a frequency as high as 1,000 kHz. However, the magnitudes of admittance signatures differed from experimental ones, the cause of which was attributed to improper damping models. Lim and Soh (2014) obtained closer match to the experimental results by adjusting material parameters and choosing a hysteretic damping model, both for the PZT and the structure.

The main advantages of coupled-field FE simulation using ANSYS^{TM} software is that the admittance signatures as those obtained experimentally can be obtained directly without the need to depend on any analytical expression. PZT is modelled as a coupled field element. An alternating voltage of 1 volt is applied across the PZT top and bottom layers by carrying out harmonic analysis. The reaction output of current flow is sought. This gives complex charge across the electrodes. The charge is suitably converted to complex current I, by differentiating it. Since $V = 1$ volt, and $Y = I / V$, I directly gives Y, the electrical admittance of the PZT chip.

3 FE simulations considered for varying PZT parameters

The objective of this numerical analysis is to study the changes in the admittance signatures (A) due to changes in the electro-mechanical material properties of the PZT chip and (B) due to changes in the geometry of the PZT chip. The admittance signatures are obtained by performing harmonic analysis in ANSYS^{TM}. Experimentally the operating frequency range to extract admittance signatures in the EMI method is usually greater than 10 kHz (Annamdas and Radhika, 2013; Annamdas and Soh, 2010). However, for this numerical simulation, to study the effects of the PZT parameter changes on admittance signatures, three different frequency ranges are considered 0–5 kHz, 20–25 kHz and 45–50 kHz. One dominant peak from each frequency range is chosen to study the pattern changes.

Figure 1 Metallic plate mounted by a piezoceramic (PZT) chip (a) 3D view (b) side-view (c) ANSYS model of the beam (see online version for colours)

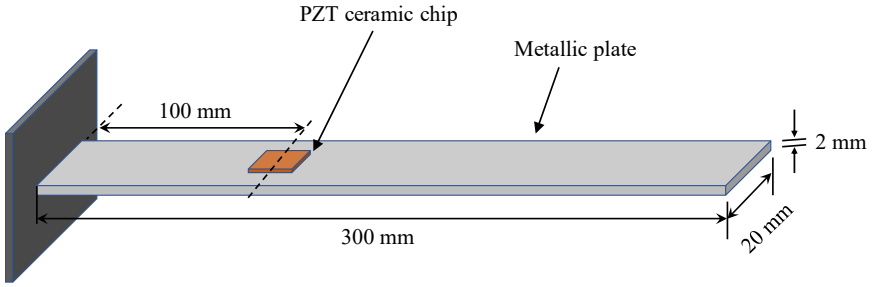

(a)

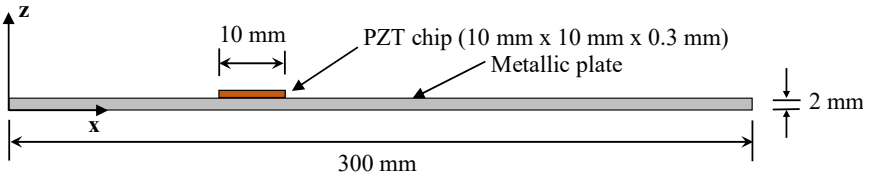

(b)

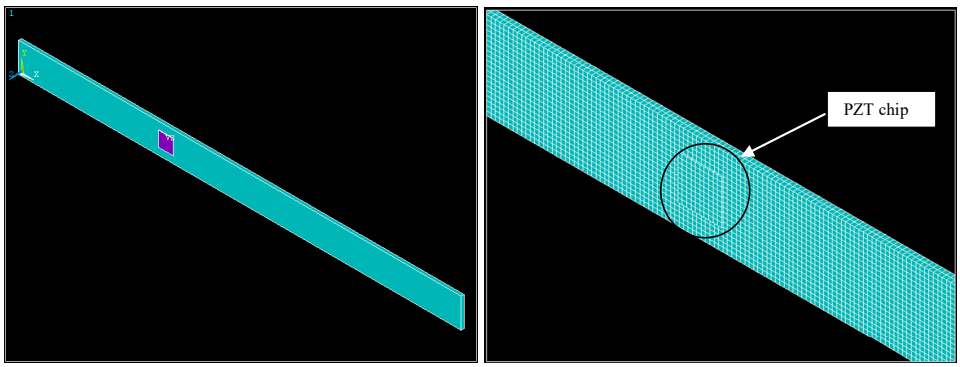

(c)

For this study, a thin metallic plate of dimensions 300 mm length, 20 mm width and 2 mm thickness, is considered as shown in the Figure 1. This is constrained at one end to form a cantilever type end conditions. The piezoelectric ceramic (PZT) chip is assumed to be bonded at 100 mm from the fixed end of the plate. The base dimensions of the PZT chip are chosen to be 10 mm length, 10 mm width and 0.3 mm thickness. The PZT chip is bonded symmetrically over the width of the top surface of the thin metallic plate as shown in the Figure 1, which also shows the ANSYS model. In this analysis, the thickness of the bonding adhesive layer is ignored and the PZT is assumed to be perfectly bonded to the structure.

The material properties considered for the PZT are based on catalogue of PI ceramic for PI 155, commonly considered in the literature, as shown in Table 1. Hysteretic damping ratio is chosen as used by Lim and Soh (2014). The properties of the metallic material of the plate are listed in Table 2.

Table 1 Properties of the piezoceramic (PZT) material (reference specimen)

Parameters	*Symbols*	*Values*	*Units*
Density	ρ	7,800	kg/m^3
Compliance	$s_{11} = s_{22}$	15	10^{-12} m^2/N
	s_{33}	19	
	$s_{12} = s_{21}$	–4.5	
	$s_{13} = s_{31}$	–5.7	
	$s_{23} = s_{32}$	–5.7	
	$s_{44} = s_{55}$	39	
	s_{66}	49.4	
Electric permittivity (relative values)	ε_{11}^T	1,980	
	ε_{22}^T	1,980	
	ε_{33}^T	2,400	
Piezoelectric strain coefficients	d_{31}	–210	10^{-12} C/N
	d_{32}	–210	
	d_{33}	500	
	d_{24}	-	
	d_{15}	580	
Mechanical quality factor	Q_m	100	
Damping ratio (hysteretic)	$\xi_{PZT} = (2Q_m)^{-1}$	0.005	
Dielectric loss tangent	tanδ	0.02	

Table 2 Properties for the host structure (metallic plate) material

Property	*Notation and value*
Young's modulus	$E = 6.89 \times 10^{10}$ N/m^2
Density	$\rho = 2{,}600$ kg/m^3
Poisson's ratio	$\nu = 0.3$
Hysteretic damping ratio	$\xi = 0.0005$

3.1 Changes in material properties of the PZT

The parameters in PZT material properties those are considered for changes are given in Table 3. Note that while one parameter of Table 3 (say density) was changed, it was ensured that all the other parameters of PZT material were retained as per Table 1.

Table 3 PZT chip material properties considered for comparative analysis

	PZT material property	*Case 1*	*Case 2*	*Case 3*	*Case 4*	*Case 5*
1	Density(D) (kg/m^3)	7,800	8,500	9,000	9,500	10,000
2	Relative Permittivity (P) (ε_{11}^T, ε_{22}^T, ε_{33}^T)	(1,800, 1,800, 2,000)	(1,980, 1,980, 2,400)	(2,200, 2,200, 2,260)	(2,400, 2,400, 2,800)	-
3	Damping ratio (DR)	0.005	0.01	0.015	0.02	-
4	Piezo-strain coefficients (PSC) (C/N)					-
	d_{31}	-180×10^{-12}	-210×10^{-12}	-240×10^{-12}	-270×10^{-12}	-
	d_{32}	-180×10^{-12}	-210×10^{-12}	-240×10^{-12}	-270×10^{-12}	-
	d_{33}	430×10^{-12}	500×10^{-12}	530×10^{-12}	560×10^{-12}	-
	d_{15}	550×10^{-12}	580×10^{-12}	610×10^{-12}	640×10^{-12}	-

3.2 Changes in geometry of the PZT

As given in Table 4, the changes in the dimensions of the PZT were considered keeping the metallic plate (host structure) dimensions constant with length 300 mm, width 20 mm and thickness 2 mm. The location of the PZT chip is also maintained the same.

Table 4 PZT chip dimensions considered for comparative analysis

Change in dimension	*Cases*					*Dimensions which remain unchanged*
	1	*2*	*3*	*4*	*5*	
Length (mm)	10	12	14	16	18	Width = 10 mm, thickness = 0.3 mm
Width (mm)	10	12	14	16	18	Length = 10 mm, thickness = 0.3 mm
Thickness (mm)	0.2	0.3	0.4	0.6	-	Length = 10 mm, width = 10 mm

4 Results and discussion

Harmonic analysis is performed, as described in Section 2, for all the cases given in Tables 3 and 4. The admittance signatures in their real and imaginary parts, i.e., conductance signatures and susceptance signatures are analysed separately.

4.1 Changes in PZT material properties

4.1.1 Changes in PZT chip densities

The conductance and susceptance signatures obtained for various cases in PZT densities are shown in Figure 2(a) and 2(b), respectively. From the signatures we can see that there is practically no change. However, we shall zoom into these signatures and observe the seventh peak of the signature at 2,938 Hz. The close view of the seventh peak both in conductance and susceptance are shown in Figures 3(a) and 3(b), respectively. It can be observed that as the PZT density increases the resonant frequency decreases, which is reflected in the peaks shifting mildly towards the left. We may note that this peak in the signatures corresponds to the natural frequency of the structural system. The natural frequencies of the PZT alone for in plane vibrations are found to be beyond 120 kHz. In general, the natural frequency of any structural system is proportional to the system stiffness or flexural rigidity and inversely proportional to the system mass. Thus, with increase in the PZT density, the system mass increases mildly and hence the natural frequencies decrease. This can be observed in the resonant peaks in the signature mildly shift towards the left. Similar pattern is observed for higher frequency ranges. As a sample, the conductance signature frequency peaks at 21.86 kHz and 45.53 kHz are presented in Figure 4. The frequency changes observed are less than 5 Hz for lower frequency range (0–5 kHz) and up to 50 Hz for the higher frequency ranges. This shows that higher frequency ranges display greater visible sensitivity to parameter changes compared to the lower ones. The frequency reductions due to local damages in the host structure are usually higher than 50 Hz, particularly at higher frequency ranges (Naidu, 2004). Thus, for the purpose of structural damage identification, the peak frequency variations due to changes in PZT densities are practically insignificant. Further, even in the event of PZT chip getting deteriorated, the density of the chip will not usually alter. Two signatures of the same PZT (fixed density) are compared at two instances for damage identification. Thus, the conclusion of this section is that higher the density of the PZT chip, the greater will be the reduction of the system natural frequencies, which are more clearly visible at higher frequency ranges. It may also be observed that there is no change in the amplitudes of the peaks in the signatures.

Figure 2 (a) Conductance (b) Susceptance signatures for varying PZT density values (frequency range: 0–5 kHz) (see online version for colours)

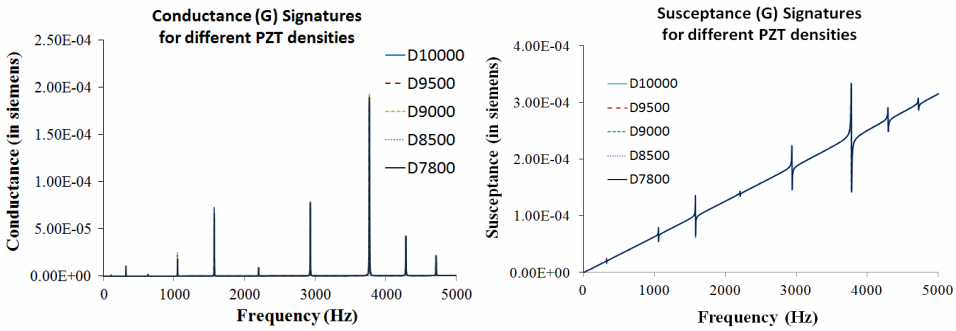

(a) (b)

Figure 3 (a) Conductance (b) Susceptance signatures for varying PZT density values (frequency range: 2.92–2.95 kHz) (see online version for colours)

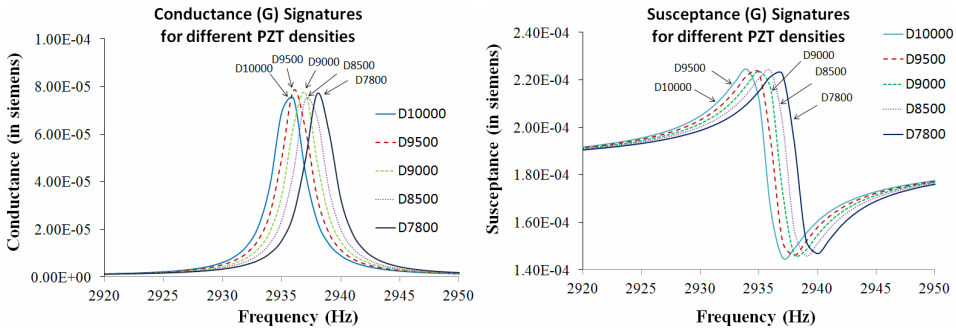

(a) (b)

Figure 4 (a) Conductance signature for varying PZT density values (21.8–21.9 kHz) (b) Conductance signature for varying PZT density values (45.4–45.6 kHz) (see online version for colours)

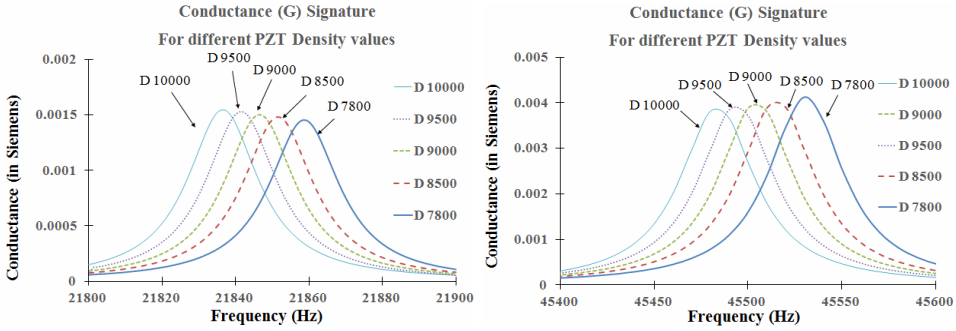

(a) (b)

4.1.2 Changes in the PZT material's relative permittivity

The conductance and susceptance signatures for this case for the frequency range of 0–5 kHz are shown in Figure 5(a) and 5(b), and for the zoomed seventh resonant peak near 2,938 Hz are shown in Figure 6(a) and 6(b). From Figure 5(a) it can be observed that the conductance signature does not show any notable change, whereas in Figure 5(b) the susceptance signatures show an increasing trend of their overall slope with increase in the relative permittivity values. This is more clearly observed in the zoomed signatures in Figure 6. The conductance signatures do not change even for higher frequency ranges. Thus, the susceptance signatures are shown around the frequencies of 21.43 kHz and 45.53 kHz in Figure 7.

Figure 5 (a) Conductance (b) Susceptance signatures for varying PZT relative permittivity values (frequency range: 0–5 kHz) (see online version for colours)

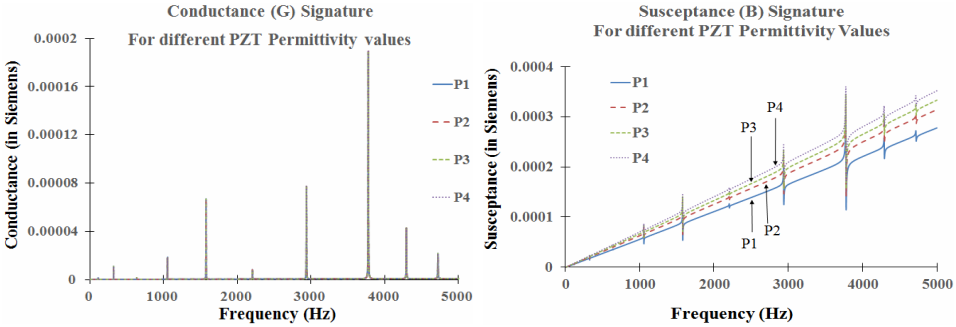

(a) (b)

Figure 6 (a) Conductance (b) Susceptance signatures for varying PZT relative permittivity values (frequency range: 2.93–2.95 kHz) (see online version for colours)

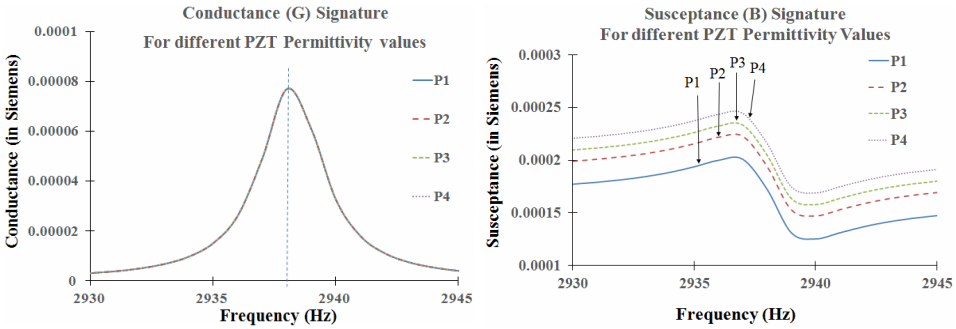

(a) (b)

Figure 7 (a) Conductance signature for varying PZT permittivity values (21.3–21.55 kHz) (b) Conductance signature for varying PZT permittivity values (45.4–45.6 kHz) (see online version for colours)

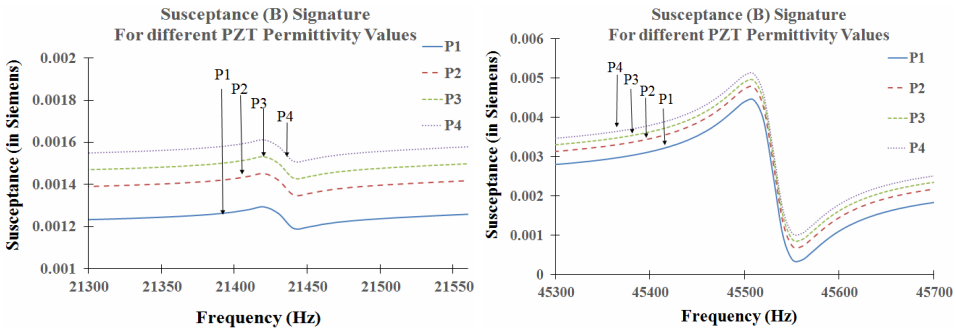

(a) (b)

It is a known fact that the resonant peaks are contributed to by the coupling of the impedances of actuator and structure, by what is called impedance matching (Liang et al., 1994b). In the simplified Liang's expression in equation (3) used for a single degree of freedom structural system, it can be observed that the relative permittivity term is independent of the impedance coupling term $\left(\frac{Z}{Z+Z_a}\right)$. Since only dielectric permittivity is increased without changing any of the other parameters, it does not effect the admittance peak amplitude.

4.1.3 Changes in the PZT material damping ratio

The conductance and susceptance signatures for this case for the frequency range of 0–5 kHz are shown in Figure 8(a) and 8(b), and for the zoomed seventh resonant peak near 2,938 Hz is shown in Figure 9(a) and 9(b). It is a well-known fact that structures damping ratio inversely affects the amplitudes of the resonant peaks in any frequency response curves. Here it may be noted that the PZT material damping ratio is increased (ref. Table 3), while the structural damping ratio is maintained constant (ref. Table 2). One clear observation is that the peaks occur at the same frequency and do not shift horizontally. Thus, the damping ratio of the PZT does not alter the system natural frequencies. From Figure 8(a) it can be observed that the conductance signature does not show any meaningful changes, except at the peaks. Similar observation is made for susceptance signatures in Figure 8(b). A closer look of the peak at 2,938 Hz in Figure 9(a) reveals that the peak amplitudes mildly decrease with the increase in damping ratio of the PZT material. Similar observations can be made from the susceptance signatures in Figure 9(b), where the amplitude of the jump decreases with the increase of the damping ratio. Similar observations are made for higher frequency ranges and conductance signatures at around the frequencies of 21.86 kHz and 45.53 kHz are presented in Figure 10. The damping ratio of the PZT is derived from mechanical quality factor which is dependent on dielectric, elastic and piezoelectric losses. The observations here are as expected. However, it may be noted that decrease in the amplitudes of peaks are negligible as these peaks correspond to the structural natural frequency and not the PZT chips individual natural frequency. If the damping of the metallic plate is altered than the peak amplitude is expected to change significantly.

Figure 8 (a) Conductance (b) Susceptance signatures for varying PZT damping ratio values (frequency range: 0–5 kHz) (see online version for colours)

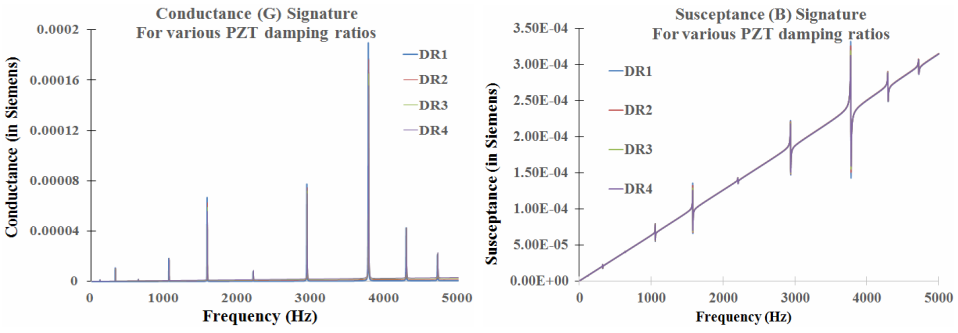

(a) (b)

Figure 9 (a) Conductance (b) Susceptance signatures for varying PZT damping ratio values (frequency range: 2.93–2.95 kHz) (see online version for colours)

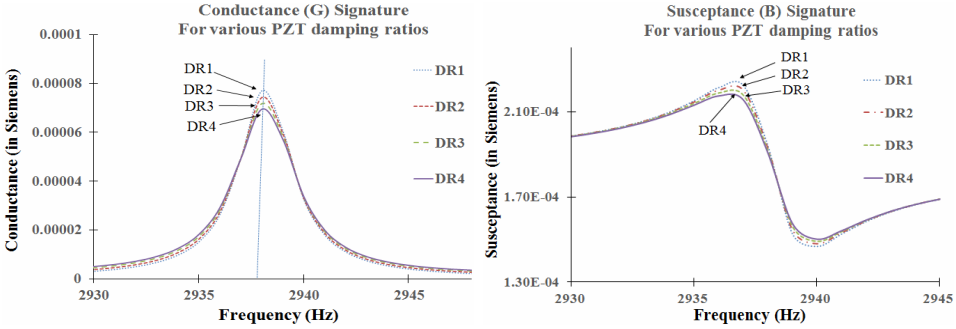

(a) (b)

Figure 10 (a) Conductance signature for varying PZT damping ratios (21.8–21.92 kHz) (b) Conductance signature for varying PZT damping ratios (45.4–45.6 kHz) (see online version for colours)

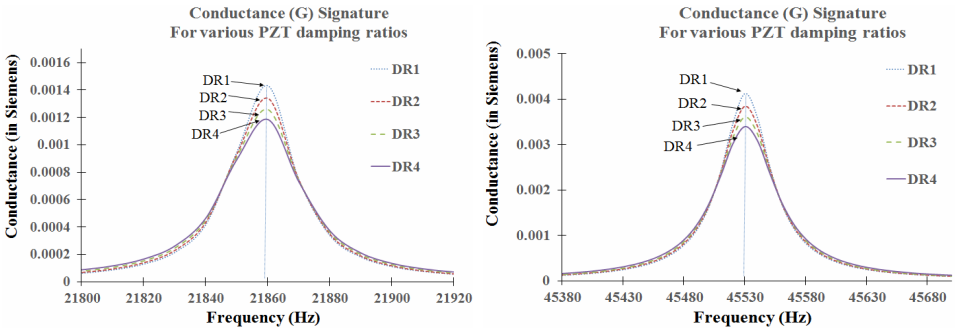

(a) (b)

4.1.4 Changes in the PZT material's strain coefficients

The conductance and susceptance signatures for this case for the frequency range of 0–5 kHz are shown in Figure 11(a) and 11(b), and for the zoomed seventh resonant peak near 2,938 Hz are shown in Figure 12(a) and 12(b). The conductance signatures in Figure 11(a) are not distinguishable. However, Figure 12(a) shows that the peak amplitudes slightly increase with increase in the piezoelectric strain coefficients. Figure 13 gives the conductance signatures at higher frequency ranges. This is easily understandable as in Liang's equation (3), we see a direct proportionality of the strain coefficient with the electrical admittance and particularly that it is also a factor of the term containing impedance coupling. Thus, the conductance signatures peak amplitudes increase with increase in strain coefficients, unlike the case for relative permittivity. However, the susceptance curves show increase in the constant overall positive slope with increase in the actuating frequency, which is similar to the case for relative permittivity values.

Figure 11 (a) Conductance (b) Susceptance signatures for varying PZT strain coefficients (frequency range: 0–5 kHz) (see online version for colours)

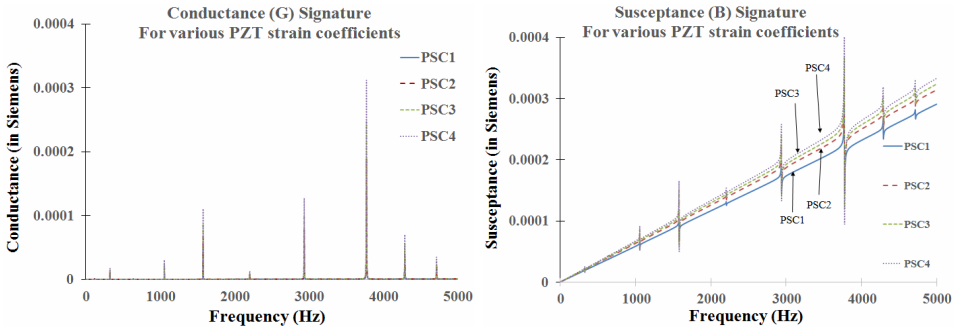

(a) (b)

Figure 12 (a) Conductance (b) Susceptance signatures for varying PZT strain coefficients (frequency range: 2.93–2.95 kHz) (see online version for colours)

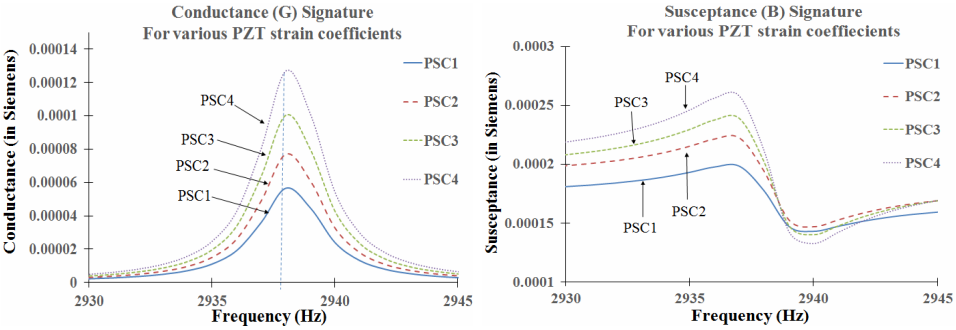

(a) (b)

Figure 13 (a) Conductance signature for varying PZT strain coefficients (21.72–21.97 kHz) (b) Conductance signature for varying PZT strain coefficients (451–45.9 kHz) (see online version for colours)

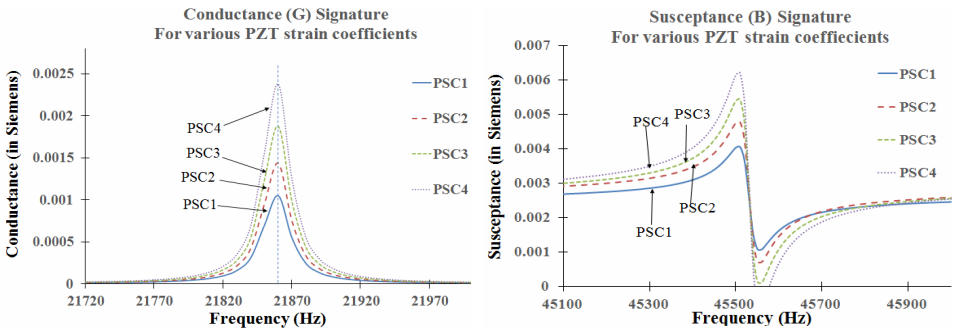

(a) (b)

4.2 Changes in PZT chip's geometry

4.2.1 Changes in the PZT chip's length

The conductance and susceptance signatures for this case for the frequency range of 0–5 kHz are shown in Figure 14(a) and 14(b), and for the zoomed seventh resonant peak near 2,938 Hz are shown in Figure 15(a) and 15(b). The conductance signatures show increase in the peak amplitudes and small horizontal rightward shift indicating a mild increase in system's natural frequencies. The susceptance signatures show increase in the constant upward slope. The changes in the susceptance signatures are more significant than the changes in the conductance signatures. It can be observed in Liang's equation (3) that the PZT length l_a is directly proportional to the admittance Y. Thus, the increase in peak amplitudes in Figure 15(a) and 15(b) are accordingly understood.

Figure 14 (a) Conductance (b) Susceptance signatures for varying PZT chip lengths (frequency range: 0–5 kHz) (see online version for colours)

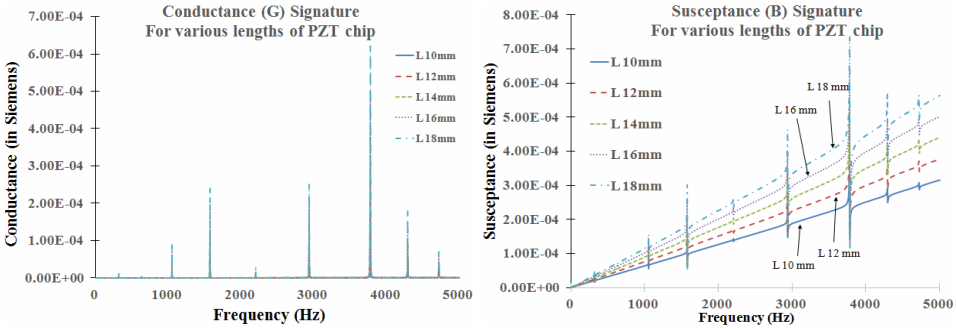

(a) (b)

Figure 15 (a) Conductance (b) Susceptance signatures for varying PZT chip lengths (frequency range: 2.92–2.95 kHz) (see online version for colours)

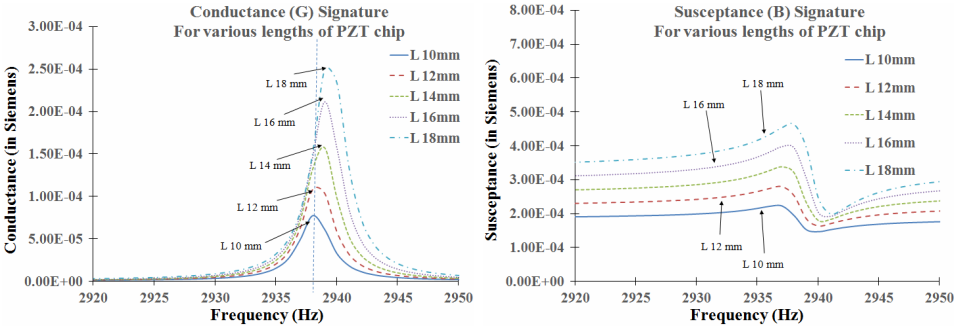

(a) (b)

4.2.2 Changes in the PZT chip's width

The conductance and susceptance signatures for this case for the frequency range of 0–5 kHz are shown in Figure 16(a) and 16(b), and for the zoomed seventh resonant peak near 2,938 Hz are shown in Figure 17(a) and 17(b). In Liang's equation (3), admittance is directly proportional also to the width of the PZT. Thus, the susceptance patterns are very similar to that observed for the case of varying lengths. However, even though the peak amplitudes in conductance signatures increase with width, the peaks show small horizontal shift towards the left, opposite to that obtained for length change.

Figure 16 (a) Conductance (b) Susceptance signatures for varying PZT chip widths (frequency range: 0–5 kHz) (see online version for colours)

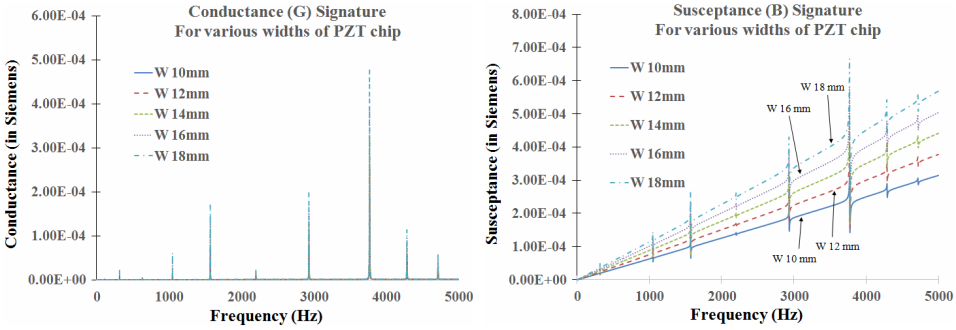

(a) (b)

Figure 17 (a) Conductance (b) Susceptance signatures for varying PZT chip widths (frequency range: 2.92–2.95 kHz) (see online version for colours)

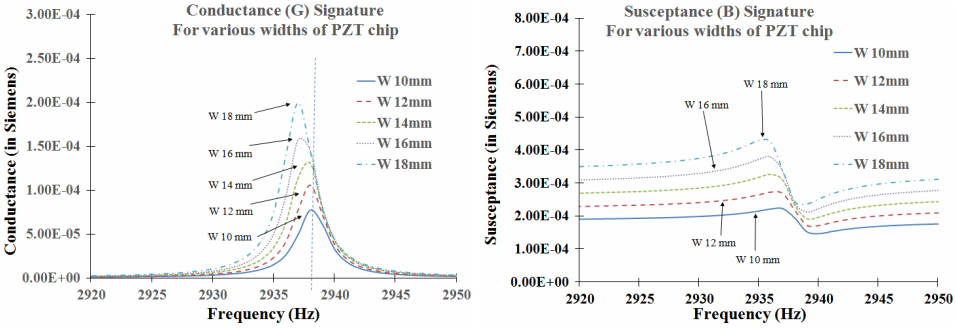

(a) (b)

4.2.3 Changes in the PZT chip's thickness

The conductance and susceptance signatures for this case for the frequency range of 0–5 kHz are shown in Figure 18(a) and 18(b), and for the zoomed seventh resonant peak near 2,938 Hz are shown in Figure 19(a) and 19(b). The conductance signatures show no

changes in the peak location, implying that the thickness of the PZT does not affect the system natural frequencies. However, the peak amplitudes of the conductance signatures decrease with the increase of the PZT thickness. The susceptance signatures, unlike the other cases, show decrease in the overall upward slope with increase in thickness. This is so because the admittance Y is inversely proportional to the thickness of the PZT, h_a, as can be observed in the Liang's equation (3).

Figure 18 (a) Conductance (b) Susceptance signatures for varying PZT chip thickness (frequency range: 0–5 kHz) (see online version for colours)

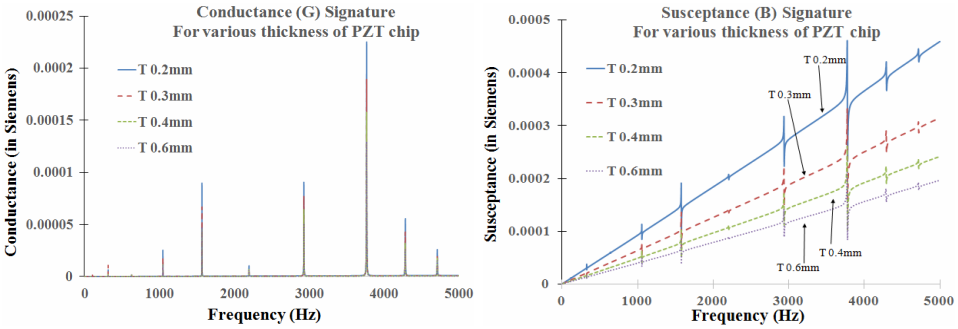

(a) (b)

It must also be noted that other peaks other than at 2,938 Hz are studied closely and show similar trends to those observed in each of the above cases. These are not presented for brevity. Another fact to note is the nature of the horizontal peak shifts due to changes in PZT chip dimensions. From the well established results on vibrations of continuous systems that the natural frequencies of the cantilever beam/plate is $\omega_{nf} \propto \sqrt{\frac{EI}{\rho AL^4}}$, where ρ, E and L are the material density, Young's modulus and longitudinal length of the cantilever.

A and I are the cross-sectional area and the moment of inertia about the neutral axis of the cross-sectional area of the plate. Addition of the PZT chip onto the system increases the system mass, stiffness and local moment of inertia. It does not change the overall length of the system.

Figure 19 (a) Conductance (b) Susceptance signatures for varying PZT chip thickness (frequency range: 2.92–2.95 kHz) (see online version for colours)

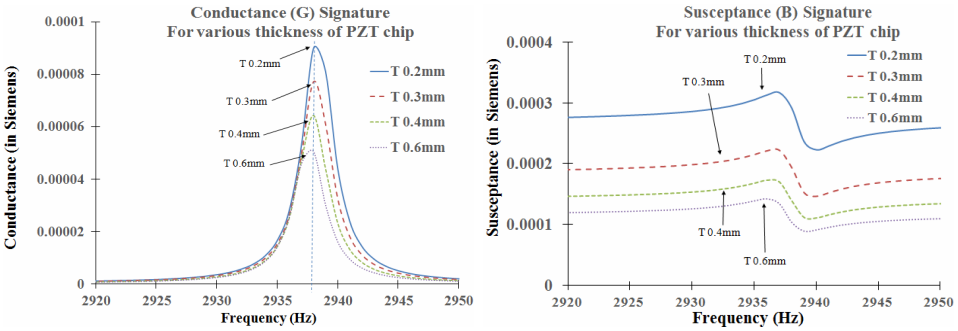

(a) (b)

At first the comparison of the plate mounted by PZT of different lengths is considered. When only the length of the PZT chip is increased alongside the length of the cantilever plate, the flexural rigidity (EI) is increased for the cross-sections over the entire length of the PZT chip which is mounted on the plate. Thus, the overall flexural rigidity of the system (EI) increases, when the PZT chip is of greater length. However, the density and local cross-sectional area remains same throughout the length of the PZT chip. Thus, as the EI term in the numerator dominates the denominator, the systems natural frequencies tend to increase and thus we observe slight rightwards tilt or shift of the peaks in the admittance signatures, as seen in Figures 15(a) and 15(b).

However, when width of the PZT chip is increased keeping length and thickness constant, the cross-sectional area in the local vicinity of the PZT chip, increases. The natural frequency, being inversely proportional to area, decreases as shown in Figure 17. Thus, we observe slight leftwards shift of the peaks in the admittance signatures. However, in both the above cases of change in length and width of the PZT chip the change in the natural frequency is very small hardly < 2 Hz, even for width and length change up to 80%.

Further, when thickness alone is increased there is no horizontal shift of the peaks, indicating that the natural frequency of the system remains unchanged, as in Figure 18. Thus, it is observed that PZT chip being relatively of a small size as compared to the host structure does not significantly alter the system natural frequency.

Table 5 Admittance signature pattern changes for increasing values of PZT parameters

S. no.	*PZT parameter (increasing values)*	*Conductance signature*		*Susceptance signature*	
		Horizontal shift	*Vertical shift*	*Horizontal shift*	*Vertical shift*
1	PZT density	Slightly to left	No	Slightly to left	No
2	Relative permittivity	No	No	No	Increases in proportion to frequency
3	Damping	No	Peaks lowered mildly	No	Downwards mild lowered
4	Piezo strain coefficients	No	Peaks increased	No	Increases in proportion to frequency
5	Length	Peaks tilt rightwards (mildly)	Peaks increased	Mild rightwards (almost nil)	Increases in proportion to frequency
6	Width	Peaks tilt leftward (mildly)	Peaks increased	Mild leftwards (almost nil)	Increases in proportion to frequency
7	Thickness	No	Peaks lowered	No	Decreases in proportion to frequency

General overall note: it is already established numerically and experimentally that actual damage in the structure causes significant and unequal horizontal shifts of the resonant

peaks in the admittance signatures (Naidu, 2004; Naidu and Soh, 2004a, 2004b). Therefore, it may be concluded from all the above observations presented in this paper that PZT parameter changes influence the admittance signatures uniformly throughout the signatures frequency range, which is quite different from the structural damage induced changes. Further, the susceptance signatures are more sensitive to the changes in the PZT material and geometric parameters, compared to the conductance signatures. This observation has be experimentally observed and recommended as well in previous works (Bhalla et al., 2003; Sun et al., 1995), which has been more elaborately studied and observed in this work. The observations of the signature pattern changes based on the present numerical study are summarised in Table 5.

5 Conclusions

In this paper, the results of a numerical study are presented to understand the influence of material and geometric parameters of the piezoelectric ceramic (PZT) chip on its electric admittance signatures, when it is surface bonded to a structure. The precise analysis of this admittance signature is the focal point of the diagnostic test in the EMI technique for SHM. It is helpful to study the pattern changes of the admittance signatures due to PZT parameters to distinguish the pattern changes due to structural damage. The coupled-field FE analysis for the EMI method has been demonstrated to give good prediction of the admittance signatures. Therefore, in this numerical study, this method has been adopted to simulate the admittance signatures in ANSYS^{TM}. The analyses showed that admittance signatures, both the real and imaginary parts, show similar pattern change uniformly throughout the signature. This is quite unlike the structural damage induced changes. It has also been observed that the susceptance signatures are more sensitive to the PZT parameter changes than the conductance signatures. Susceptance signatures can therefore be analysed to monitor the condition of the PZT chip. The specific pattern changes corresponding to the specific PZT properties have be presented. This study shall be very useful for signal pattern recognition for effective diagnostics in SHM applications using the EMI technique. The conclusions noted here may be useful for further study on damage identification.

References

Adhikari, S. and Bhalla, S. (2018) 'Modified dual piezo configuration for improved structural health monitoring using electro-mechanical impedance (EMI) technique', *Exp. Tech.*, pp.1–16.

Annamdas, V.G. and Radhika, M.A. (2013) 'Electromechanical impedance of piezoelectric transducers for monitoring metallic and non-metallic structures: a review of wired, wireless and energy-harvesting methods', *J. Intell. Mater. Syst. Struct.*, Vol. 24, No. 9, pp.1021–1042.

Annamdas, V.G.M. and Soh, C.K. (2007) 'Three-dimensional electromechanical impedance model. I: formulation of directional sum impedance', *J. Aerosp. Eng.*, Vol. 20, No. 1, pp.53–62.

Annamdas, V.G.M. and Soh, C.K. (2010) 'Application of electromechanical impedance technique for engineering structures: review and future issues', *J. Intell. Mater. Syst. Struct.*, Vol. 21, pp.41–59.

Bhalla, S. (2004) *A Mechanical Impedance Approach for Structural Identification, Health Monitoring and Non-Destructive Evaluation using Piezo-Impedance Transducers*, PhD thesis, Nanyang Technological University, Singapore.

Bhalla, S. and Moharana, S. (2013) 'A refined shear lag model for adhesively bonded piezo-impedance transducers', *J. Intell. Mater. Syst. Struct.*, Vol. 24, No. 1, pp.33–48.

Bhalla, S. and Soh, C.K. (2004a) 'Structural health monitoring by piezo-impedance transducers. I: modeling', *J. Aerosp. Eng.*, Vol. 17, No. 4, pp.154–165.

Bhalla, S. and Soh, C.K. (2004b) 'Structural health monitoring by piezo-impedance transducers. II: applications', *J. Aerosp. Eng.*, Vol. 17, No. 4, pp.166–175.

Bhalla, S. and Soh, C.K. (2004c) 'Electromechanical impedance modeling for adhesively bonded piezo-transducers', *J. Intell. Mater. Syst. Struct.*, Vol. 15, No. 12, pp.955–972.

Bhalla, S., Naidu, A.S. and Soh, C.K. (2003) 'Influence of structure-actuator interactions and temperature on piezoelectric mechatronic signatures for NDE', in *Smart Materials, Structures, and Systems. International Society for Optics and Photonics*, Proc. SPIE 5062, pp.263–269.

Boller, C. and Meyendorf, N. (2008) 'State-of-the-art in structural health monitoring for aeronautics', in *Proc. of Internat. Symposium on NDT in Aerospace*, Citeseer.

Brownjohn, J.M. (2007) 'Structural health monitoring of civil infrastructure', *Philos. Trans. R. Soc. Lond. Math. Phys. Eng. Sci.*, Vol. 365, No. 1851, pp.589–622.

Chang, F-K. (1999) *Structural Health Monitoring 2000*, Taylor & Francis, USA.

Diamanti, K. and Soutis, C. (2010) 'Structural health monitoring techniques for aircraft composite structures', *Prog. Aerosp. Sci.*, Vol. 46, No. 8, pp.342–352.

Djemana, M. and Hrairi, M. (2016) 'Modelling and simulation of impedance-based damage monitoring of structures', *Int. J. Simul. Model.*, Vol. 15, No. 3, pp.395–408.

Fairweather, J.A. (1998) *Designing with Active Materials: an Impedance based Approach*, PhD thesis, Rensselaer Polytechnic Institute, New York.

Fan, S., Li, W., Kong, Q., Feng, Q. and Song, G. (2018a) 'Monitoring of pin connection loosening using eletromechanical impedance: numerical simulation with experimental verification', *J. Intell. Mater. Syst. Struct.*, Vol. 29, No. 9, pp.1964–1973.

Fan, S., Zhao, S., Qi, B. and Kong, Q. (2018b) 'Damage evaluation of concrete column under impact load using a piezoelectric-based EMI technique', *Sensors*, Vol. 18, No. 5, p.1591.

Fan, X., Li, J., Hao, H. and Ma, S. (2018c) 'Identification of minor structural damage based on electromechanical impedance sensitivity and sparse regularization', *J. Aerosp. Eng.*, Vol. 31, No. 5, p.4018061.

Farrar, C.R. and Worden, K. (2007) 'An introduction to structural health monitoring', *Philos. Trans. R. Soc. Lond. Math. Phys. Eng. Sci.*, Vol. 365, No. 1851, pp.303–315.

Giurgiutiu, V. and Zagrai, A.N. (2000) 'Characterization of piezoelectric wafer active sensors', *J. Intell. Mater. Syst. Struct.*, Vol. 11, No. 12, pp.959–976.

Giurgiutiu, V. and Zagrai, A.N. (2002) 'Embedded self-sensing piezoelectric active sensors for on-line structural identification', *Trans.-Am. Soc. Mech. Eng. J. Vib. Acoust.*, Vol. 124, No. 1, pp.116–125.

Hoła, J. and Schabowicz, K. (2010) 'State-of-the-art non-destructive methods for diagnostic testing of building structures – anticipated development trends', *Arch. Civ. Mech. Eng.*, Vol. 10, No. 3, pp.5–18.

Lalande, F. (1995) *Modeling of the Induced Strain Actuation of Shell Structures*, PhD dissertation, Virginia Polytechnic Institute and State University, Blacksburg, VA.

Li, W., Fan, S., Ho, S.C.M., Wu, J. and Song, G. (2017) 'Interfacial debonding detection in fiber-reinforced polymer rebar-reinforced concrete using electro-mechanical impedance technique', *Struct. Health Monit.*, Vol. 17, No. 3, pp.461–471.

Liang, C., Sun, F. and Rogers, C. (1994a) 'An impedance method for dynamic analysis of active material systems', *J. Vib. Acoust.*, Vol. 116, No. 1, pp.120–128.

Liang, C., Sun, F. and Rogers, C. (1994b) 'Coupled electro-mechanical analysis of adaptive material systems – determination of the actuator power consumption and system energy transfer', *J. Intell. Mater. Syst. Struct.*, Vol. 5, No. 1, pp.12–20.

Lim, Y.Y. (2007) *Health Monitoring of Civil Structures using Piezoelectric Materials*, MEngg thesis, Nanyang Technological University, Singapore.

Lim, Y.Y. and Soh, C.K. (2012) 'Effect of varying axial load under fixed boundary condition on admittance signatures of electromechanical impedance technique', *J. Intell. Mater. Syst. Struct.*, Vol. 23, No. 7, pp.815–826.

Lim, Y.Y. and Soh, C.K. (2014) 'Towards more accurate numerical modeling of impedance based high frequency harmonic vibration', *Smart Mater. Struct.*, Vol. 23, No. 3, p.35017.

Liu, P., Wang, W., Chen, Y., Feng, X. and Miao, L. (2017) 'Concrete damage diagnosis using electromechanical impedance technique', *Constr. Build. Mater.* Vol. 136, pp.450–455.

Liu, W. and Giurgiutiu, V. (2007) 'Finite element simulation of piezoelectric wafer active sensors for structural health monitoring with coupled-filed elements', in *International Society for Optics and Photonics (SPIE) The 14th International Symposium on: Smart Structures and Materials & Nondestructive Evaluation and Health Monitoring*, pp.65293R–65293R.

Lu, X., Lim, Y.Y. and Soh, C.K. (2017) 'A novel electromechanical impedance-based model for strength development monitoring of cementitious materials', *Struct. Health Monit.*, Vol. 17, No. 4, pp.902–918.

Madhav, A.V.G. and Soh, C.K. (2007) 'An electromechanical impedance model of a piezoceramic transducer-structure in the presence of thick adhesive bonding', *Smart Mater. Struct.*, Vol. 16, No. 3, p.673.

Malinowski, P., Wandowski, T. and Ostachowicz, W. (2015) 'The use of electromechanical impedance conductance signatures for detection of weak adhesive bonds of carbon fibre-reinforced polymer', *Struct. Health Monit.*, Vol. 14, pp.332–344.

Min, J., Yun, C-B. and Hong, J-W. (2016) 'An electromechanical impedance-based method for tensile force estimation and damage diagnosis of post-tensioning systems', *Smart Struct. Syst.*, Vol. 17, No. 1, pp.107–122.

Na, W.S. and Baek, J. (2018) 'A review of the piezoelectric electromechanical impedance based structural health monitoring technique for engineering structures', *Sensors*, Vol. 18, No. 5, p.1307.

Naidu, A.S.K. (2004) *Structural Damage Identification with Admittance Signatures of Smart PZT Transducers*, PhD thesis, Nanyang Technological University, Singapore.

Naidu, A.S.K. and Soh, C.K. (2004a) 'Identifying damage location with admittance signatures of smart piezo-transducers', *J. Intell. Mater. Syst. Struct.*, Vol. 15, No. 8, pp.627–642.

Naidu, A.S.K. and Soh, C.K. (2004b) 'Damage severity and propagation characterization with admittance signatures of piezo transducers', *Smart Mater. Struct.*, Vol. 13, No. 2, p.393.

Park, G., Sohn, H., Farrar, C.R. and Inman, D.J. (2003) 'Overview of piezoelectric impedance-based health monitoring and path forward', *Shock Vib. Dig.*, Vol. 35, No. 6, pp.451–464.

Park, S., Kim, J-W., Lee, C. and Park, S-K. (2011) 'Impedance-based wireless debonding condition monitoring of CFRP laminated concrete structures', *NDT E Int.*, Vol. 44, No. 2, pp.232–238.

Roth, W. and Giurgiutiu, V. (2017) 'Structural health monitoring of an adhesive disbond through electromechanical impedance spectroscopy', *Int. J. Adhes. Adhes.*, March, Vol. 73, pp.109–117.

Sohn, H., Farrar, C.R., Hemez, F.M., Shunk, D.D., Stinemates, D.W., Nadler, B.R. and Czarnecki, J.J. (2004) *A Review of Structural Health Monitoring Literature: 1996–2001*, Los Alamos National Laboratory Los Alamos, NM.

Song, H., Lim, H.J. and Sohn, H. (2013) 'Electromechanical impedance measurement from large structures using a dual piezoelectric transducer', *J. Sound Vib.*, Vol. 332, No. 25, pp.6580–6595.

Sun, F.P., Chaudhry, Z.A., Rogers, C.A., Majmundar, M. and Liang, C. (1995) Automated real-time structure health monitoring via signature pattern recognition', in *'Smart Structures & Materials' 95, International Society for Optics and Photonics*, Proc. SPIE 2443, pp.236–247.

Talakokula, V., Bhalla, S. and Gupta, A. (2018) 'Monitoring early hydration of reinforced concrete structures using structural parameters identified by piezo sensors via electromechanical impedance technique', *Mech. Syst. Signal Process.*, January, Vol. 99, pp.129–141.

Tinoco, H.A., Robledo-Callejas, L., Marulanda, D.J. and Serpa, A.L. (2016) 'Damage detection in plates using the electromechanical impedance technique based on decoupled measurements of piezoelectric transducers', *J. Sound Vib.*, December, Vol. 384, pp.146–162.

Wang, D., Li, Z. and Zhu, H. (2016) 'A new three-dimensional electromechanical impedance model for an embedded dual-PZT transducer', *Smart Mater. Struct.*, Vol. 25, No. 7, p.75002.

Xu, Y.G. and Liu, G.R. (2002) 'A modified electro-mechanical impedance model of piezoelectric actuator-sensors for debonding detection of composite patches', *J. Intell. Mater. Syst. Struct.*, Vol. 13, No. 6, pp.389–396.

Yan, W. and Chen, W.Q. (2010) 'Structural health monitoring using high-frequency electromechanical impedance signatures', *Adv. Civ. Eng*, p.11, Article ID 429148.

Yang, Y., Lim, Y.Y. and Soh, C.K. (2008) 'Practical issues related to the application of the electromechanical impedance technique in the structural health monitoring of civil structures: II. Numerical verification', *Smart Mater. Struct.*, Vol. 17, No. 3, p.35009.

Zagrai, A.N. and Giurgiutiu, V. (2001a) 'Electro-mechanical impedance method for crack detection in thin plates', *J. Intell. Mater. Syst. Struct.*, Vol. 12, No. 10, pp.709–718.

Zagrai, A.N. and Giurgiutiu, V. (2001b) 'Electro-mechanical impedance method for crack detection in thin wall structures', *3rd Int. Workshop Struct. Health Monit.*, pp.12–14.

Zagrai, A.N. and Giurgiutiu, V. (2001c) 'The electro-mechanical impedance method for damage identification in circular plates', Presented at *142nd Meeting of Acoustical Society of America*, Fort Lauderdale, Florida, 3–7 December.

Zhou, S.W., Liang, C. and Rogers, C.A. (1996) 'An impedance-based system modeling approach for induced strain actuator-driven structures', *J. Vib. Acoust.*, Vol. 118, No. 3, pp.323–331.